

Supporting Information for ”Development of topography in 3D continental collision models”

A. E. Pusok,¹ Boris J. P. Kaus¹

Contents of this file

1. S1. Scaling analysis
2. Figures S1 to S2
3. Table S1

Corresponding author: A. E. Pusok, Institute of Geosciences, Johannes Gutenberg University, J.-J.-Becher-Weg 21, Mainz, D-55128, Germany. (puesoek@uni-mainz.de)

¹Institute of Geosciences, Johannes Gutenberg University, Mainz, Germany.

S1. Scaling analysis

S1.1. Mountain building processes

To form mountain ranges, horizontal forces must be applied to lithospheric plates, to drive them together and to cause crustal shortening and thickening. Isostatic compensation of the thickened crust then buoys up the mountain range to form high topographic amplitudes relative to the lowlands. When crustal shortening occurs, the forces driving the material together do work against resistive stresses, mainly against gravity. Thus the formation of both mountains and crustal roots is associated with an increase in gravitational potential energy, and part of the work done by forces that drive the plates together creates that potential energy.

S1.1.1. Gravitational potential energy

The potential energy is defined as the line integral of a force causing displacement integrated along the component of displacement:

$$\int \vec{F} \cdot d\vec{s}. \quad (\text{S1})$$

We consider the potential energy stored in a column of material of unit cross-sectional area, which is the potential energy per unit surface of the earth (Fig. S1a) [*Molnar and Lyon-Caen*, 1988; *Schmalholz et al.*, 2014; *England and McKenzie*, 1982; *Turcotte and Schubert*, 2002]. The vertical force per unit area is the product of gravity, density, and thickness of the overlying layer (ρgh). Work is done against such a force in the vertical direction. The potential energy per unit area of a column of material above a given depth

can be calculated as the integral of the lithostatic pressure from the Earth's surface to that depth.

If the compensation depth is taken at a certain depth in the mantle ($z = H_0 + \Delta H + h_m$), the lithostatic pressure in the lowlands, $P_L(z)$, is given by:

$$P_L(z) = \rho_c g H_0 + \rho_m g (\Delta H + h_m) \quad (\text{S2})$$

where ρ_c and ρ_m are the densities of the crust and mantle, assumed constant here, and H_0 is the crustal thickness. In a mountainous region or a plateau with an elevation of h and a crustal root extending to a depth ΔH beneath the normal crustal thickness H_0 , the lithostatic pressure, $P_M(z)$ can be written as:

$$P_M(z) = \rho_c g (h + H_0 + \Delta H) + \rho_m g h_m \quad (\text{S3})$$

with $-h \leq 0 \leq H_0 + \Delta H + h_m$. Isostatic compensation requires that the lithostatic pressure at depth $z = H_0 + \Delta H$ is constant, and $P_L = P_M$, therefore, $\Delta \rho \Delta H = \rho_c h$, where $\Delta \rho = \rho_m - \rho_c$.

The difference in potential energy per unit area beneath the mountains and lowlands is:

$$\begin{aligned} \Delta GPE &= \int_{-h}^{H_0 + \Delta H + h_m} [P_M(z) - P_L(z)] dz \quad (\text{S4}) \\ &= \rho_c g h \left(\frac{h}{2} + H_0 + \Delta H + h_m \right) \\ &\quad - \Delta \rho g \Delta H \left(\frac{\Delta H}{2} + h_m \right) \end{aligned}$$

Considering the depth of compensation at the bottom of the crustal root ($z = H_0 + \Delta H$), the change in potential energy between mountains and lowlands becomes:

$$\Delta GPE = \rho_c g h \left(\frac{h}{2} + H_0 + \Delta H \right) - \Delta \rho g \frac{\Delta H^2}{2} \quad (\text{S5})$$

$$= \rho_c g h \left(\frac{h}{2} + H_0 + \frac{\Delta H}{2} \right).$$

S1.1.2. Change in GPE per unit length

Molnar and Lyon-Caen [1988] explored further the considerations for gravitational potential energy in the formation of mountain ranges. They showed that when the forces driving the plates together can no longer supply the energy needed to elevate a high range or a plateau higher, the mountain range is likely to grow laterally in width instead of increasing in height. This can be shown with a simple mathematical argument.

As shown previously, the potential energy created in a crustal layer displaced horizontally by an amount d , such that a mountain range of width w and height h forms (Eq. 5), is given by:

$$\Delta GPE(w, h, d) = \rho_c g w h \left(\frac{h}{2} + H_0 + \frac{\Delta H}{2} \right). \quad (\text{S6})$$

If there is a further displacement d , such that the total displacement is $2d$, *Molnar and Lyon-Caen* [1988] note that there are 2 possibilities for deformation: one in which the elevation could increase to $2h$ and the thickness of root would increase to $2\Delta H$, or another when the width increases to $2w$. In the first case, the potential energy per unit length is:

$$\Delta GPE(w, 2h, 2d) = 2\rho_c g w h (h + H_0 + \Delta H). \quad (\text{S7})$$

And in the second, is:

$$\Delta GPE(2w, h, 2d) = 2\rho_c g w h \left(\frac{h}{2} + H_0 + \frac{\Delta H}{2} \right). \quad (\text{S8})$$

The difference in potential energy per unit length of a range created by doubling its width from that created by doubling its height is:

$$\delta GPE = \Delta GPE(w, 2h, 2d) - \Delta GPE(2w, h, 2d) \quad (\text{S9})$$

$$\begin{aligned}
&= \rho_c g w h (h + \Delta H) \\
&= \frac{\rho_c \rho_m}{\Delta \rho} g w h^2.
\end{aligned}$$

Equation (9) shows that due the square dependence on h , more work must be done to increase the range in height than laterally.

A similar reasoning can be done to illustrate that shortening a half-width area $w/2$ to elevate it to a height h , requires half the energy required to elevate an area of width w . This suggests that extra energy is available to elevate the mountain range of width $w/2$ by at least 50% more ($> 1.5h$).

$$\Delta GPE(w/2, 1.5h) = \frac{3}{4} \rho_c g w h \left(\frac{3h}{4} + H_0 + \frac{3\Delta H}{4} \right). \quad (\text{S10})$$

Then the difference in potential energy per unit length is:

$$\begin{aligned}
\delta GPE &= \Delta GPE(w, h) - \Delta GPE(w/2, 1.5h) \\
&= \rho_c g w h \left(\frac{7H_0}{16} - \frac{h}{16} - \frac{\Delta H}{16} \right) \\
&= \rho_c g w h \left(\frac{7H_0}{16} - \frac{h}{16} \left(1 + \frac{\rho_c}{\Delta \rho} \right) \right) > \frac{h}{4} > 0
\end{aligned} \quad (\text{S11})$$

The inequality in (11) is true for natural parameters, for example, if one assumes that $H_0 > 2h$ and that $(1 + \frac{\rho_c}{\Delta \rho}) < 10$, which are reasonable assumptions for crustal geometries and materials. We explore the importance of this inequality, due to its connection to shortening a homogeneous layer versus shortening a heterogeneous layer (i.e. with strong crustal blocks). In the presence of heterogenous crustal blocks, less material is available for deformation (i.e. shorter width), the energy has a finite space for propagation, and we can expect further uplift, compared to a homogenous layer case. This will be seen later in simulation results with or without the presence of strong blocks.

S1.1.3. Resisting stresses

Viscous forces also resist the deformation driven by the compressional forces. In a viscous medium, these stresses can be approximated as:

$$\sigma = 2\eta\dot{\epsilon} \sim 2\eta\frac{u_0}{L} \quad (\text{S12})$$

where L is a characteristic length, $\dot{\epsilon}_0 = \frac{u_0}{L}$ is the characteristic strain rate of the system, η_0 is the viscosity of the crustal material and u_0 is the horizontal convergence velocity.

S1.1.4. Maximum height

As seen before, it is more favourable to propagate higher amplitudes laterally than vertically. Therefore, for a given driving force, the mountain range will not necessarily reach a higher elevation. Instead, the mountain range should reach a limiting elevation and crustal thickness before the energy starts spreading laterally, regardless of how strong the materials constituting them. The maximum elevation of a mountain range for a certain applied force, is found from:

$$\rho_c g h \left(\frac{h}{2} + H_0 + \frac{\rho_c h}{2\Delta\rho} \right) = 2\eta \frac{u_0}{L} d \quad (\text{S13})$$

$$\frac{1}{2}\rho_c g h^2 \left(1 + \frac{\rho_c}{\Delta\rho} \right) + \rho_c g H_0 h - 2\eta \frac{u_0}{L} d = 0 \quad (\text{S14})$$

The last equation is a quadratic equation in h of the form $ah^2 + bh + c = 0$, where the maximum elevation can be calculated as:

$$h_{max} = \frac{b}{2a} = \frac{\Delta\rho}{\rho_m} H_0 \quad (\text{S15})$$

S1.2. Argand number

Based on the above considerations, *England and McKenzie* [1982] defined the Argand number, which is the ratio between an estimate of the excess pressure arising from a crustal thickness contrast of order L and the stress required to deform the medium at a strain rate characteristic of the system:

$$Ar = \frac{P(L)}{\tau(\dot{\epsilon}_0)} \quad (\text{S16})$$

where $P(L)$ is the excess pressure in the system and $\tau(\dot{\epsilon}_0)$ is the viscous resistive stresses at the characteristic strain rate.

The Argand number predicts that at high values, the excess pressure will dominate and the material will flow due to pressure gradients, while for a low Argand number, the viscous stresses are high and can sustain higher pressures and higher elevations. As such, the Argand number can be interpreted as a measure of the competition between two processes: relaxation in the vertical plane due to buoyancy forces which tends to produce a plane strain situation, and a horizontal flow controlled by the geometry and the boundary conditions in the horizontal plane.

However, different formulations of the Argand number can be found in the published literature, depending on the complexity assumed in models and the definition of the characteristic length scale, L : original formulation for power-law rheology [*England and McKenzie*, 1982], plastic rheology [*Vilotte et al.*, 1986], temperature formulation [*England and Houseman*, 1989], or more recently, a buoyancy formulation [*Bajolet et al.*, 2013]. The Argand number was also applied to other phenomena such as salt tectonics [*Fernandez and Kaus*, 2014]. Moreover, some authors have used a variation of the Argand number, called the Ramberg number, Rm [*Weijermars and Schmeling*, 1986; *Medvedev*, 2002].

The Argand number was calculated here using different choices of the characteristic length scale, L , as defined in the literature: the initial thickness of the lithosphere $L = H_0$, the indenting distance $L = W_0 - W_f$, and the width of the continental indenter $L = W_0$ [Vilotte *et al.*, 1986]. Despite the different choices, all formulations show the same trend. Moreover, we note that formulations that contain only initial values [England and McKenzie, 1982] have a greater advantage over those that need information about the final stages of evolution (i.e. Bajolet *et al.* [2013]). This suggests that initial conditions prior to collision already allows prediction of the outcome of the simulation. Therefore, we keep with the original formulation from England and McKenzie [1982], where the Argand number for a viscous material is given by:

$$Ar = \frac{\rho_c g H_0 (1 - \frac{\rho_c}{\rho_m})}{\eta (u_0 / H_0)} \quad (S17)$$

where $\dot{\epsilon}_0 = u_0 / H_0$ is the characteristic strain rate, η is the effective viscosity, ρ_c and ρ_m are the densities of the crust and mantle, u_0 characteristic velocity (convergence velocity), H_0 thickness of lithosphere, and g is the gravitational acceleration.

S1.2.1. Gravitational flow

When the forces driving convergence and sustaining mountain growth are removed or diminished (as a result of slab break-off), the system will try to minimize the excess of potential energy. In this case, the material will flow laterally by gravitational flow, and we show that the topographic amplitude decreases exponentially with time. Let us consider an elevated area of radius r as in Fig. S1b, surrounded by lowlands, with a difference in height of h . The compensation depth is taken at $z = H_0$. The upward and downward

force acting on the flanks of the mountains are:

$$F_{up} = p_M A = \rho_c g (H_0 + h) \pi r^2 \quad (\text{S18})$$

$$F_{down} = p_L A = \rho_c g H_0 \pi r^2$$

Therefore, the net buoyancy force is:

$$F_{buoy} = F_{up} - F_{down} = \rho_c g h \pi r^2. \quad (\text{S19})$$

The viscous resistance acts to hamper the fast lateral collapse of the flanks. The viscous resistance in a cylinder can be approximated as:

$$\begin{aligned} F_{res} &= \tau \times 2\pi r H_0 & (\text{S20}) \\ &= 2\eta \dot{\epsilon} \times 2\pi r H_0 \\ &\sim 4\pi H_0 \eta u_o \end{aligned}$$

From the force balance, $F_{buoy} = F_{res}$, we have:

$$\frac{u_o}{h} = \frac{\rho g r^2}{4\eta H_0}. \quad (\text{S21})$$

The time dependence of h can be determined from the continuity equation [*England and McKenzie, 1982*]:

$$\frac{\partial u}{\partial t} = -\nabla \cdot (hu) \quad (\text{S22})$$

Combining the last 2 equations, it follows that:

$$\frac{u_o}{h} = \frac{\rho g r^2}{4\eta H_0} = -\frac{1}{h} \frac{\partial h}{\partial t} \quad (\text{S23})$$

Integrating, we obtain an exponential decay of h with time t :

$$h = h_0 e^{-\frac{\rho_c g r^2 t}{4\eta H_0}} \quad (\text{S24})$$

where h_0 is the maximum amplitude before gravitational flow. Equation S24 can be rewritten as:

$$h = h_0 e^{-\frac{t}{t_r}} \quad (\text{S25})$$

where t_r , the characteristic time for exponential relaxation of the flanks, is given by:

$$t_r = \frac{4\eta H_0}{\rho_c g r^2} \quad (\text{S26})$$

S2. Initial buoyancy ratio

Fig. S2 shows the evolution of topographic amplitude during homogenous shortening for different densities of the crust. The evolution of topographic amplitude is given by [Turcotte and Schubert, 2002]:

$$h = H_0 \left(1 - \frac{\rho_c}{\rho_m}\right) (\beta - 1) \quad (\text{S27})$$

$$\beta = \frac{W_0}{W}$$

where β is the compression factor and is the ratio between the initial width and the current width, H_0 is the initial thickness, ρ_c is the density of the crust, and ρ_m is the density of the mantle. Fig. S2 shows that with increasing compression (or with time if compressional forces are kept constant), the topographic amplitude of a lighter crust increases faster than for a denser crust. This phenomenon is also observed in our numerical results, that simulations with a lighter crust that are subjected to compression, will develop higher topographic amplitudes on average compared to simulations with a less dense crust.

S3. Numerical simulations

Parameters for the simulations displayed in figures are given in Table S1.

References

- Bajolet, F., A. Replumaz, and R. Lainé (2013), Orocline and syntaxes formation during subduction and collision, *Tectonics*, *32*, 1–18, doi:10.1002/tect.20087.
- England, P., and G. A. Houseman (1989), Extension During Continental Convergence, with Application to the Tibetan Plateau, *Journal of Geophysical Research*, *94*(B12), 17,561–17,579, doi:10.1029/JB094iB12p17561.
- England, P., and D. McKenzie (1982), A Thin Viscous Sheet Model for Continental Deformation, *Geophys. J. R. astr. Soc.*, *70*, 295–321, doi:10.1111/j.1365-246X.1982.tb04969.x.
- Fernandez, N., and B. J. P. Kaus (2014), Fold interaction and wavelength selection in 3D models of multilayer detachment folding, *Tectonophysics*, *632*, 199–217, doi:10.1016/j.tecto.2014.06.013.
- Medvedev, S. (2002), Mechanics of viscous wedges: Modeling by analytical and numerical approaches, *Journal of Geophysical Research*, *107*(B6), doi:10.1029/2001JB000145.
- Molnar, P., and H. Lyon-Caen (1988), Some Simple Physical Aspects of the Support, Structure, and Evolution of Mountain Belts, *Geological Society of America Special Paper*, *218*, 179–207.
- Schmalholz, S. M., S. Medvedev, S. M. Lechmann, and Y. Podladchikov (2014), Relationship between tectonic overpressure, deviatoric stress, driving force, isostasy and gravitational potential energy, *Geophysical Journal International*, *197*(2), 680–696, doi:10.1093/gji/ggu040.
- Turcotte, D. L., and G. Schubert (2002), *Geodynamics*, 2nd ed., Cambridge University Press.

Vilotte, J. P., R. Madariaga, M. Daignieres, and O. C. Zienkiewicz (1986), Numerical Study of Continental Collision: Influence of Buoyancy Forces and an Initial Stiff Inclusion, *Geophys. J. R. astr. Soc.*, *84*, 279–310, doi:10.1111/j.1365-246X.1986.tb04357.x.

Weijermars, R., and H. Schmeling (1986), Scaling of newtonian and non newtonian fluid dynamics without inertia for quantative modelling of rock flow due to gravity (including the concept of rheological similarity), *Phys. Earth Planet. Inter.*, *43*, 938–954.

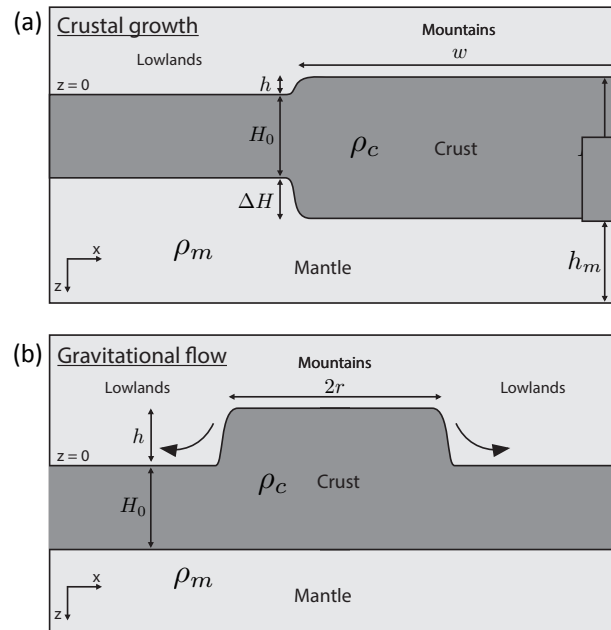


Figure S1. a) Sketch of building gravitational potential energy in mountain building. b) Sketch of forces during gravitational flow.

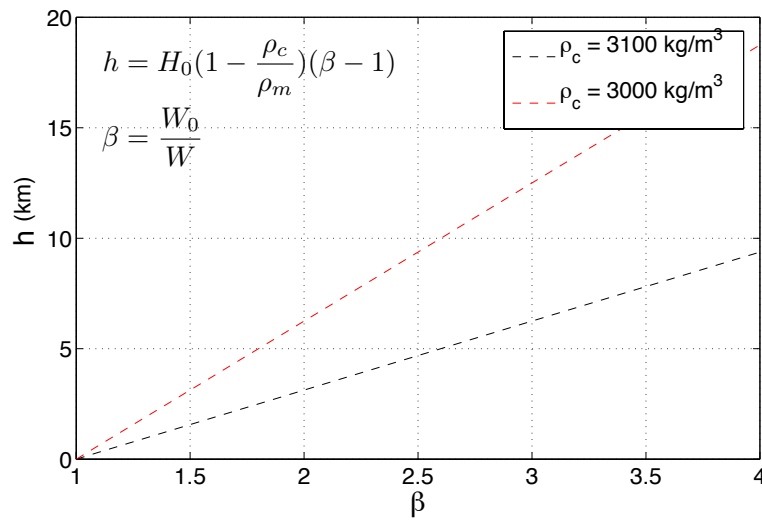


Figure S2. Topographic amplitude growth during homogenous shortening. h represents topography amplitude in km, and β represents the compression factor and is the ratio between the initial width and the current width. Calculations are done for two crustal densities to show that for a lighter crust, topographic amplitude increases faster during shortening compared for the case with a denser crust.

| Parameter values displayed in the figures | | | | | | | | | | | | | |
|---|--------------|--------------|-------------|-------------|--------------|--------------|-------------|-------------|--------------|--------------|-------------|-------------|---------|
| Simulation | ρ_{OUM} | η_{OUM} | ρ_{OC} | η_{OC} | ρ_{IUM} | η_{IUM} | ρ_{IC} | η_{IC} | ρ_{AUM} | η_{AUM} | ρ_{AC} | η_{AC} | Forcing |
| B00 | 3300 | 1e23 | 3200 | 1e20 | 3100 | 1e23 | 3100 | 5e20 | 3000 | 1e22 | 3000 | 1e22 | FS |
| C00 (ref) | 3300 | 1e23 | 3200 | 1e20 | 3100 | 1e23 | 3100 | 5e20 | 3000 | 1e21 | 3000 | 1e22 | FS |
| SBB00 | 3300 | 1e23 | 3200 | 1e20 | 3100 | 1e23 | 3100 | 5e20 | 3000 | 1e22 | 3000 | 1e22 | SB |
| P5B00 | 3300 | 1e23 | 3200 | 1e20 | 3100 | 1e23 | 3100 | 5e20 | 3000 | 1e22 | 3000 | 1e22 | EF |
| SBP5B00 | 3300 | 1e23 | 3200 | 1e20 | 3100 | 1e23 | 3100 | 5e20 | 3000 | 1e22 | 3000 | 1e22 | EF+SB |
| SBP5UPA01 | 3300 | 1e23 | 3100 | 1e20 | 3100 | 1e23 | 3100 | 5e20 | 3000 | 1e21 | 3000 | 1e21 | EF+SB |
| SBP5UPA08 | 3300 | 1e23 | 3100 | 1e20 | 3100 | 1e23 | 3100 | 5e20 | 3100 | 1e21 | 3100 | 1e21 | EF+SB |
| SBP5UPA29 | 3300 | 1e23 | 3100 | 1e20 | 3100 | 1e23 | 3100 | 5e20 | 3000 | 1e23 | 3000 | 1e23 | EF+SB |
| SBP5UPA36 | 3300 | 1e23 | 3100 | 1e20 | 3100 | 1e23 | 3100 | 5e20 | 3100 | 1e23 | 3100 | 1e23 | EF+SB |

Table S1. Parameters table for the simulations displayed in figures. Each phase has 2 properties: density (ρ) and viscosity (η). Values are in $[\rho] = \text{kg/m}^3$ and $[\eta] = \text{Pa.s}$. Phases: OUM - Oceanic Upper Mantle Lithosphere, OC - Oceanic Crust, IUM - Indentor Upper Mantle Lithosphere, IC - Indentor Crust, AUM - Asian Upper Mantle Lithosphere, AC - Asian Crust. In addition, the properties of the asthenospheric mantle ($\rho_m = 3200 \text{ kg/m}^3$, $\eta_m = 1e20 \text{ Pa.s}$), the air ($\rho_{air} = 0 \text{ kg/m}^3$, $\eta_{air} = 1e18 \text{ Pa.s}$) and lower mantle ($\rho_{LM} = 3250 \text{ kg/m}^3$, $\eta_{LM} = 1e21 \text{ Pa.s}$) are the same for all simulations. Symbols in the right column mean: FS - free subduction, SB - with strong blocks ($\rho_{SB} = 3100 \text{ kg/m}^3$, $\eta_{SB} = 5e23 \text{ Pa.s}$) and EF - external forcing with $V_{push} = 5 \text{ cm/yr}$. Due to the small number of models displayed in this paper, the nomenclature of all models is as follows: 1) a set of simulations with FS are labeled A, B, C and represent simulations where slab and continental indentor parameters were tested, 2) another set of simulations with FS are labeled UPA, UPB, UPC in which upper plate parameters were tested, and 3) simulations with EF just have an additional prefix SB for strong blocks and/or P5 for pushing with $V_{push} = 5 \text{ cm/yr}$.